

1 **Tissue nonspecific alkaline phosphatase improves bone**
2 **quality but does not alleviate craniosynostosis in the**
3 **FGFR2^{C342Y/+} mouse model of Crouzon syndrome**

4

5 Hwa Kyung Nam^{1#}, Sara Dean Schutte^{1#}, Nan E. Hatch^{1*}

6

7 ¹ Department of Orthodontics and Pediatric Dentistry, School of Dentistry, University of
8 Michigan, Ann Arbor, Michigan, United States of America

9

10 * Corresponding author
11 E-mail: nhatch@umich.edu
12

13 # These authors contributed equally to this work.

14

15

16

17

18

19

20 **Abstract**

21 Crouzon syndrome is a congenital disorder characterized by craniosynostosis, the premature
22 fusion of cranial bones. Craniosynostosis leads to high intracranial pressure and abnormal skull
23 and facial shapes that are relieved by surgery. Crouzon syndrome is caused by activating
24 mutations in fibroblast growth factor receptor 2 (FGFR2). The goal of this study was to
25 determine if delivery of recombinant tissue nonspecific alkaline phosphatase (TNAP) could
26 prevent or diminish the severity of craniosynostosis in post-natal craniosynostosis onset BALB/c
27 and/or peri-natal craniosynostosis onset C57BL/6 FGFR2^{C342Y/+} mouse models of Crouzon
28 syndrome. Mice were injected with a lentivirus encoding a mineral targeted form of TNAP
29 immediately after birth. Cranial bone fusion as well as cranial bone volume, mineral content
30 and density were assessed by micro computed tomography. Craniofacial shape was measured
31 with calipers using previously established landmarks and measurements. Alkaline phosphatase
32 activity levels were measured in serum. Results show that postnatal delivery of TNAP increases
33 serum levels of alkaline phosphatase activity and improves bone volume, density and mineral
34 content, but does not alleviate craniosynostosis, craniofacial shape or cranial base
35 abnormalities in FGFR2^{C342Y/+} Crouzon mice. These results indicate that post-natal recombinant
36 TNAP enzyme therapy is therapeutic for bone mineralization but not efficacious for relief of
37 FGFR-associated craniosynostosis and associated craniofacial shape defects.

38

39 **Introduction**

40 Craniosynostosis is the pediatric condition of premature cranial bone fusion. This condition
41 can lead to high intracranial pressure, abnormal skull and facial shapes, blindness, seizures and
42 brain abnormalities [1-6]. Because the sole treatment is surgery, even with appropriately early
43 diagnosis patients can suffer high morbidity [7-9]. Surgical approaches also do not fully correct
44 abnormal skull and facial shapes, which contribute to social challenges. Previous studies
45 showed that the pathogenesis of craniosynostosis can include abnormal boundary
46 formation/maintenance, lineage commitment, proliferation and/or apoptosis of cranial
47 progenitor cells [10-23]. Despite these important advancements, a pharmaceutical treatment
48 for craniosynostosis is not yet realized.

49 Craniosynostosis occurs in association with activating mutations in *Fgfr2* [10, 12, 24, 25].
50 Craniosynostosis also occurs at high incidence in infants with hypophosphatasia, a metabolic
51 disorder that occurs due to inactivating mutations in *Alpl*, the gene for tissue nonspecific
52 alkaline phosphatase (TNAP) [26-29]. We previously demonstrated that FGF signaling decreases
53 TNAP expression [14, 30, 31]. TNAP expression is also reduced in primary cells isolated from
54 FGFR2^{C342Y/+} mice that have been induced to differentiate into osteoblasts when cultured *in*
55 *vitro* or in a 3D collagenous matrix *in vivo* [14, 15]. These results indicate that one of the
56 mechanisms by which FGF signaling influences craniofacial skeletal development may involve
57 reduced TNAP. Notably, postnatal delivery of a recombinant mineral-targeted form of TNAP did
58 prevent craniosynostosis in the TNAP^{-/-} mouse model of hypophosphatasia [32]. The objective
59 of this study was to determine if postnatal delivery of recombinant TNAP could prevent or
60 diminish the severity of craniosynostosis and associated craniofacial shape defects in the
61 FGFR2^{C342Y/+} mouse model of Crouzon syndrome.

62

63 **Materials and methods**

64 **TNAP Lentivirus**

65 Recombinant mineral-targeted TNAP lentivirus was generously provided by Dr. Jose Luis Millán
66 (Sanford Burnham Prebys Medical Discovery Institute, La Jolla, CA). This virus expresses a
67 mineral-targeted protein that is composed of soluble human TNAP enzyme fused to the
68 constant region of human IgG1 and a C-terminal deca-aspartate motif to confer targeting to
69 hydroxyapatite. The aspartate tag confers 30x higher affinity for hydroxyapatite than untagged
70 enzyme [33]. Production and titer of the lentivirus was performed by the University of Michigan
71 Vector Core. Treatment with this recombinant form of TNAP was previously shown to increase
72 serum alkaline phosphatase levels and rescue long bone and craniofacial defects seen in
73 hypophosphatasia [26, 32, 34, 35].

74

75 **Animal Procedures**

76 Because severity of craniosynostosis and associated craniofacial shape defects are variable on
77 the mixed genetic background, $FGFR2^{C342Y/+}$ mice were backcrossed with BALB/c and C57BL/6
78 mice (obtained from Charles River Laboratories) for at least fifteen generations prior to
79 experiments. BALB/c $FGFR2^{C342Y/+}$ mice have a moderate form of Crouzon syndrome with
80 craniosynostosis apparent between three and four weeks after birth [15]. C57BL/6 mice have a
81 severe form of Crouzon syndrome with craniosynostosis first apparent in neonatal mice (data not
82 shown). Genotyping was performed as previously described [12, 15]. Briefly, DNA from tail

83 digests was amplified by polymerase chain reaction using 5'-gagtaccatgctgactgcatgc-3' and 5'-
84 ggagaggcatctctgtttcaagacc-3' primers to yield a 200 base pair band for wild type FGFR2 and a 300
85 base pair band for mutant FGFR2^{C342Y}. Mice were fed ad libitum and housed under standard 12
86 hour dark/light cycles. Litters were randomly assigned to treatment/no treatment groups.
87 Treated mice were injected with 1.0×10^7 transforming units lentivirus or an equivalent volume
88 of phosphate buffered saline via the jugular vein two days after birth. BALB/c mice (n=12 FGFR2^{+/+}
89 control mice, n=14 FGFR2^{C342Y/+} control mice, n=16 FGFR2^{C342Y/+} TNAP lentivirus treated mice)
90 were euthanized by CO₂ overdose at four weeks post-natal and C57BL/6 mice (n=7 FGFR2^{+/+}
91 control mice, n=7 FGFR2^{C342Y/+} control mice, n=14 FGFR2^{C342Y/+} TNAP lentivirus treated mice) were
92 euthanized by CO₂ overdose at three weeks post-natal for analyses. BALB/c mice were sacrificed
93 at a later age than C57BL/6 mice because craniosynostosis onset occurs later in BALB/C than in
94 C57BL/6 FGFR2^{C342Y/+} mice. Blood was collected by aortic puncture under surgical anesthesia.
95 Mice were weighed, and body length was measured for each animal. All animal procedures were
96 prospectively approved of by the University of Michigan's University Committee on Use and Care
97 of Animals (UCUCA, protocol PRO00006815). All samples were de-identified as to genotype and
98 treatment group, and each analysis was performed on all BALB/c mice or on all C67BL/6 mice at
99 one time. The primary outcome assessment was craniosynostosis incidence. Secondary outcome
100 assessments included cranial bone density measurements, craniofacial shape measurements,
101 cranial base synchondrosis fusions and cranial base bone lengths.

102

103 **Serum Analyses**

104 Mice were fasted for six hours prior to blood collection. Alkaline phosphatase activity (AP) in
105 serum was quantified using the colorimetric reagent 4-nitrophenyl-phosphate disodium
106 hexahydrate (Sigma), as compared to a standard curve using commercially available alkaline
107 phosphatase enzyme (Sigma). Inorganic phosphate quantifications were performed using
108 commercially available kits (Pointe Scientific), also as compared to standard curves.

109

110 **Micro Computed Tomography**

111 Whole skulls were scanned at an 18 μm isotropic voxel resolution using the eXplore Locus SP
112 micro-computed tomography imaging system (GE Healthcare Pre-Clinical Imaging, London, ON,
113 Canada). Regions of interest (ROI's) for parietal and frontal bones were established as 1 mm in
114 length, 1 mm in width and depth equivalent to thickness of bone, as previously described [15,
115 29]. Density, volume and mineral content of cranial bones from mice were measured using
116 previously established methods using Microview version 2.2 software (GE Healthcare Pre-Clinical
117 Imaging, London, ON) and established algorithms [36, 37].

118

119 **Cranial Suture Assessment**

120 Fusion between cranial bones (fusion of coronal suture, lambdoid suture and sagittal suture) plus
121 fusion of the inter-sphenoidal (ISS) and spheno-occipital (SOS) synchondroses were identified on
122 micro CT scans of skulls dissected mice. Cranial sutures were viewed using the two-dimensional
123 micro CT slices in an orthogonal view across the entire length of the suture or synchondrosis, as
124 previously described [15, 29].

125 Reliability of suture fusion assessment was verified by both intra-operator and inter-
126 operator reliability statistics by calculating intraclass correlation coefficients (ICC). Intra-
127 operator reliability statistics was carried out by assessing suture fusion status of the coronal,
128 sagittal and lambdoid sutures as well as the inter-sphenoidal (ISS) and spheno-occipital (SOS)
129 synchondroses on fifteen micro CT scans by one investigator two times separated by a two-
130 month period. Inter-operator reliability was carried out by analyzing fifteen micro CT scans by a
131 second investigator. The ICC for intraoperator reliability for suture fusion assessment is .970
132 ($p \leq .0001$) and the ICC for interoperator reliability is .972 ($p \leq .0001$). Thus, there is high
133 intraoperator and interoperator reliability for suture fusion assessment.

134

135 **Linear Measurements**

136 Craniofacial linear skeletal measurements were taken using digital calipers on dissected skulls.
137 Linear measurements were calculated using previously reported craniofacial skeletal landmarks
138 [15, 38, 39], including standard measurements currently in use by the Craniofacial Mutant Mouse
139 Resource of Jackson Laboratory (Bar Harbor, ME). Linear measurements were normalized to total
140 skull length (measured from nasale to opisthion) to account for size differences between
141 $FGFR2^{+/+}$ and $FGFR2^{C342Y/+}$ mice. Measurements were performed twice and an average of the two
142 measurements was utilized for statistical comparison by genotype and treatment. Cranial base
143 anterior-posterior bone lengths were measured on micro CT scans using *Dolphin Imaging 11.0*
144 software (Dolphin Imaging and Management Solutions, Chatsworth, CA), as previously described
145 [40].

146

147 **Statistics**

148 An Analysis of Variance (ANOVA) was performed to compare groups by gender, genotype and
149 treatment group. Because serum AP levels varied in mice injected with the lentivirus, linear
150 regressions were also performed to determine if, and to what extent serum AP levels
151 associated with changes in measured phenotypes. The incidence of cranial suture fusion, and
152 cranial base synchondrosis fusion was analyzed by the Fishers exact test.

153

154 **Results**

155 Injection with the TNAP expression lentivirus significantly increased serum alkaline phosphatase
156 (AP) levels in all of the treated mice (Table 1). BALB/c Crouzon mice injected with the lentivirus
157 increased serum AP levels by 1.2 U/mL when compared to control Crouzon mice ($p < .0001$)
158 when measured at four weeks old. C57BL/6 Crouzon mice injected with the TNAP expression
159 lentivirus increased serum AP levels by 1.8 U/mL when compared to control Crouzon mice
160 ($p < .0001$) when measured at three weeks old. No significant difference in serum AP levels were
161 seen between untreated Crouzon and wild type mice on the BALB/c or C57BL/6 backgrounds.
162 As expected, injection with the lentivirus did not alter serum inorganic phosphate (P_i) levels.

163 Initial statistical comparison of groups by ANOVA showed that Crouzon mice weigh less and
164 are shorter in body length than their wild type littermates, regardless of genetic background
165 (Table 1). Linear regression performed to account for serum AP level variability in the lentivirus
166 injected mice showed that, on the BALB/c background, serum AP levels did not alter weight in

167 wild type mice but did decrease weight in Crouzon mice by 0.9 g per U/ml which accounted for
168 37% of the weight variability in in these mice ($p < .03$). On the C57BL/6 background, linear
169 regression showed no impact of serum AP level on weight, regardless of genotype. Serum AP
170 levels did not alter body length, regardless of genetic background or genotype.

171 **Table 1.** Serum and Body Measurements in TNAP vs. untreated Balb/C and C57Bl/6mice.

Strain	Genotype	Treatment	Body Weight (g)	Body Length (mm)	Serum AP Level (units/ml)	Serum Pi Level (mg/dl)
Balb/C	FGFR2 ^{+/+}	no	13.5 +/- 2.2*	7.4 +/- 0.3*	0.03 +/- 0.01	10.9 +/- 0.8
Balb/C	FGFR2 ^{C342Y/+}	no	9.2 +/- 1.7	6.5 +/- 0.3	0.03 +/- 0.78	9.9 +/- 1.4
Balb/C	FGFR2 ^{C342Y/+}	yes	8.9 +/- 2.6	6.5 +/- 0.7	1.30 +/- 0.54 [#]	9.8 +/- 1.1
C57Bl/6	FGFR2 ^{+/+}	no	8.7 +/- 0.1*	6.9 +/- 0.3*	0.01 +/- 0.01	9.5 +/- 1.0
C57Bl/6	FGFR2 ^{C342Y/+}	no	5.8 +/- 1.1	5.8 +/- 0.6	0.02 +/- 0.01	8.7 +/- 1.1
C57Bl/6	FGFR2 ^{C342Y/+}	yes	6.6 +/- 1.0	5.9 +/- 0.4	1.93 +/- 0.77 [#]	9.0 +/- 0.6

172

173

* p value < 0.01 between genotypes

174

[#] p value < 0.01 between treatment groups

175

176

Qualitative analysis of craniofacial skeletal shape suggested that Crouzon mice differ in

177 morphology from their wild type counterparts, and that post-natal delivery of mineral-targeted

178 TNAP via lentivirus did not impact morphology (Figs 1,2). Craniofacial skeletal linear

179 measurements normalized to total skull length revealed many differences between FGFR2^{C342Y/+}

180 Crouzon and FGFR2^{+/+} wild type mice on both congenic backgrounds (Table 2). BALB/c Crouzon

181 mice had increased cranial height, cranial width, inner canthal distance, parietal bone length

182 and cranial height to width ratios, with decreased nasal bone length. C57BL/6 Crouzon mice

183 had increased cranial height, cranial width, inner canthal distance, frontal bone length, parietal

184 bone length and cranial height to width ratios, with decreased nose and nasal bone lengths.

185 Treatment with the TNAP lentivirus did not alter craniofacial skeletal measurements in Crouzon
 186 mice on either genetic background.

187 **Table 2.** Linear Craniofacial Skeletal Measurements in
 188 TNAP vs. untreated BALB/c and C57Bl/6 mice.

Strain	Measurement	FGFR2 ^{+/+} vehicle	FGFR2 ^{C342Y/+} vehicle	FGFR2 ^{C342Y/+} TNAP
BALB/c	Cranial Height	.36 +/- .01*	.45 +/- .01	.45 +/- .01
BALB/c	Cranial Width	.55 +/- .01*	.63 +/- .01	.62 +/- .01
BALB/c	Inner Canthal Distance	.20 +/- .01*	.25 +/- .01	.26 +/- .01
BALB/c	Nose Length	.65 +/- .01	.65 +/- .01	.65 +/- .01
BALB/c	Nasal Bone Length	.33 +/- .02*	.32 +/- .01	.32 +/- .03
BALB/c	Frontal Bone length	.33 +/- .02	.33 +/- .01	.34 +/- .03
BALB/c	Parietal Bone Length	.20 +/- .01*	.25 +/- .02	.26 +/- .01
BALB/c	Ratio Height to Width	.66 +/- .02*	.72 +/- .02	.72 +/- .02
C57Bl/6	Cranial Height	.38 +/- .01*	.52 +/- .01	.52 +/- .03
C57Bl/6	Cranial Width	.55 +/- .01*	.64 +/- .01	.64 +/- .02
C57Bl/6	Inner Canthal Distance	.23 +/- .01*	.29 +/- .01	.29 +/- .01
C57Bl/6	Nose Length	.65 +/- .01*	.62 +/- .01	.63 +/- .03
C57Bl/6	Nasal Bone Length	.32 +/- .01*	.23 +/- .02	.23 +/- .01
C57Bl/6	Frontal Bone length	.35 +/- .01*	.40 +/- .02	.41 +/- .03
C57Bl/6	Parietal Bone Length	.22 +/- .01*	.26 +/- .02	.27 +/- .02
C57Bl/6	Ratio Height to Width	.38 +/- .01*	.52 +/- .01	.52 +/- .03

189 Measures are reported as normalized to total skull length.

190 * p value < 0.01 between genotypes

191 # p value < 0.01 between treatment groups

192 Analysis of cranial bone fusions revealed high incidences of premature fusion of the coronal
 193 and lambdoid sutures in both BALB/c and C57Bl/6 Crouzon mice, with no fusions evident in
 194 wild type mice (Fig. 3). Although 100% of BALB/c and C57Bl/6 Crouzon mice exhibited coronal
 195 suture fusion, fusions in BALB/c mice tended to be point fusions as opposed to fusion of
 196 approximately 1/3 of the coronal suture in the C57Bl/6 C mice. Analysis of cranial base
 197 synchondrosis fusions also revealed high incidences of fusion of the inter-sphenoidal

198 synchondrosis (ISS) in both strains of Crouzon mice, with no fusions evident in wild type mice.
199 The incidence of fusion of the spheno-occipital synchondrosis (SOS) was higher in C57BL/6
200 Crouzon mice than BALB/c Crouzon mice, despite the younger age of the C57BL/6 mice. No
201 cranial base fusions were evident in the wild type littermate mice. While some trends, including
202 diminished incidence of lambdoid suture fusion and increased incidence of spheno-occipital
203 synchondrosis (SOS) fusion are seen upon treatment, these differences were not statistically
204 significant. Measurement of cranial base bones demonstrated decreased length of the basis-
205 sphenoid and pre-sphenoid bones in BALB/c and C57BL/6 Crouzon as compared to wild type
206 mice (Table 3). Treatment with TNAP did not increase length of the basis-sphenoid bone in
207 Crouzon mice. Treatment with TNAP did increase length of the pre-sphenoid bone in BALB/c
208 Crouzon mice, but not to the equivalent of sphenoid bone length seen in wild type mice.
209 Together, the data indicates that delivery of mineral-targeted TNAP via lentivirus shortly after
210 birth does not impact cranial bone or cranial base bone fusions in these mice. Treatment with
211 the mineral-targeted TNAP may enhance growth of anterior cranial base bones in the model of
212 more moderate Crouzon syndrome (BALB/c strain), but not to the extent seen in control wild
213 type mice.

214

215

216

217

218

219

220 **Table 3.** Cranial base measurements in TNAP vs. untreated Balb/C and C57Bl/6 mice.

221

222

223

224

Strain	Genotype	Treatment	Basis Occipitus (mm)	Basis Sphenoid (mm)	Pre-Sphenoid (mm)
Balb/C	FGFR2 ^{+/+}	vehicle	3.1 +/- 0.1	2.9 +/- 0.1*	2.5 +/- 0.1*
Balb/C	FGFR2 ^{C342Y/+}	vehicle	2.9 +/- 0.3	2.4 +/- 0.3	1.8 +/- 0.1
Balb/C	FGFR2 ^{C342Y/+}	TNAP	2.9 +/- 0.2	2.5 +/- 0.3	1.9 +/- 0.1#
C57Bl/6	FGFR2 ^{+/+}	vehicle	2.8 +/- 0.2	2.9 +/- 0.2*	2.2 +/- 0.1*
C57Bl/6	FGFR2 ^{C342Y/+}	vehicle	2.8 +/- 0.1	2.7 +/- 0.1	1.7 +/- 0.1
C57Bl/6	FGFR2 ^{C342Y/+}	TNAP	3.0 +/- 0.2	2.6 +/- 0.1	1.7 +/- 0.1

225

226

227

228

229

230

231

232

233

234

235 * p value < 0.01 between genotypes

236 # p value < 0.01 between treatment groups

237

238 Micro CT based analyses of cranial bones demonstrated significantly diminished bone

239 mineral density, tissue mineral content, tissue mineral density and bone volume fraction in

240 frontal bones, plus significantly diminished tissue mineral density and bone volume fraction in

241 parietal bones of Crouzon mice when compared to wild type littermates on both BALB/c and

242 C57BL/6 backgrounds (Table 4). Injection with the TNAP lentivirus significantly increased

243 frontal bone mineral density, tissue mineral content and bone volume fraction, plus parietal

244 bone volume fraction in Crouzon mice on the BALB/c background. Injection with the TNAP

245 lentivirus did not significantly impact any of the cranial bone parameters in Crouzon mice on

246 the C57BL/6 background.

247

248

249

250

251
252

Table 4. Cranial bone volume, density and mineral content in TNAP vs. untreated congenic BALB/c and C57BL/6 mice.

Strain	Genotype	Treatment	Cranial Bone	Bone Mineral Content (mg)	Bone Mineral Density (mg/cc)	Tissue Mineral Content (mg)	Tissue Mineral Density (mg/cc)	Bone Volume Fraction
BALB/c	FGFR2 ^{+/+}	PBS	Frontal	.035 +/- .004	405 +/- 14*	.028 +/- .007*	692 +/- 14*	0.41 +/- .03*
BALB/c	FGFR2 ^{C342Y/+}	PBS	Frontal	.031 +/- .008	361 +/- 63	.020 +/- .006 [#]	671 +/- 18	0.36 +/- .0
BALB/c	FGFR2 ^{C342Y/+}	TNAP	Frontal	.035 +/- .005	401 +/- 26 [#]	.026 +/- .015 [#]	683 +/- 29	0.42 +/- .06 [#]
BALB/c	FGFR2 ^{+/+}	PBS	Parietal	.034 +/- .004	405 +/- 12	.023 +/- .005	693 +/- 15*	0.43 +/- .03*
BALB/c	FGFR2 ^{C342Y/+}	PBS	Parietal	.031 +/- .007	396 +/- 39	.020 +/- .005	669 +/- 24	0.36 +/- .06
BALB/c	FGFR2 ^{C342Y/+}	TNAP	Parietal	.034 +/- .006	403 +/- 27	.025 +/- .012	691 +/- 36	0.42 +/- .07 [#]
C57BL/6	FGFR2 ^{+/+}	PBS	Frontal	.017 +/- .003	245 +/- 25*	.006 +/- .001*	570 +/- 18*	0.12 +/- .01*
C57BL/6	FGFR2 ^{C342Y/+}	PBS	Frontal	.013 +/- .002	209 +/- 25	.004 +/- .001	519 +/- 26	0.10 +/- .01
C57BL/6	FGFR2 ^{C342Y/+}	TNAP	Frontal	.016 +/- .004	225 +/- 30	.004 +/- .001	553 +/- 40	0.11 +/- .01
C57BL/6	FGFR2 ^{+/+}	PBS	Parietal	.015 +/- .001	237 +/- 19	.005 +/- .001	590 +/- 13*	.121 +/- .023*
C57BL/6	FGFR2 ^{C342Y/+}	PBS	Parietal	.012 +/- .003	217 +/- 18	.004 +/- .001	558 +/- 36	.098 +/- .006
C57BL/6	FGFR2 ^{C342Y/+}	TNAP	Parietal	.013 +/- .004	232 +/- 42	.004 +/- .001	575 +/- 32	.105 +/- .009

253
254
255

* p value < 0.01 between genotypes
p value < 0.01 between treatment groups

256

257 Discussion

258 In this study we sought to determine if treatment with recombinant mineral targeted TNAP
259 could rescue the craniofacial skeletal phenotype of FGFR2^{C342Y/+} Crouzon mice when delivered
260 post-natal with lentivirus. The FGFR2^{C342Y/+} mutation was previously demonstrated to cause
261 ligand independent signaling and is therefore widely considered to be an activating mutation
262 leading to increased FGF signaling [41-44]. We pursued this investigation because we previously
263 demonstrated that FGF signaling diminishes TNAP expression [14, 30, 31], and showed that

264 TNAP deficiency in mice leads to a similar craniofacial phenotype to that seen in $FGFR2^{C342Y/+}$
265 Crouzon mice including coronal and lambdoid but not sagittal craniosynostosis, fusion of cranial
266 base synchondroses and abnormal brachycephalic/acrocephalic head shapes [12, 15, 29, 40].
267 Additionally, in a previous study using archival aliquots of lentivirus expressing the mineral
268 targeted recombinant form of TNAP that resulted in increases in serum AP activity in only a
269 small number of the treated mice, we found statistical differences in the morphology of the
270 inferior skull surface and skull height in treated vs. untreated $FGFR2^{C342Y/+}$ mice [45].

271 Here we found that post-natal lentiviral delivery of recombinant TNAP rescued cranial bone
272 density, mineral content and volume fraction but not craniosynostosis or craniofacial shape in
273 $FGFR2^{C342Y/+}$ Crouzon mice. Improvement of cranial bone density, mineral content and volume
274 fraction by TNAP treatment in the Crouzon mice is consistent with results showing that
275 recombinant mineral targeted TNAP treatment rescues mineralization of craniofacial and long
276 bones in in the $Alpl^{-/-}$ mouse model of infantile HPP and humans with infantile and childhood
277 HPP [32, 34, 46, 47]. Treatment with mineral targeted TNAP via lentivirus did not rescue
278 craniosynostosis or craniofacial shape defects in the Crouzon mice. This result is inconsistent
279 with the rescue of craniosynostosis seen in $Alpl^{-/-}$ mice treated with mineral targeted
280 recombinant TNAP protein [32] but is consistent with results in human studies which indicate
281 that post-natal treatment with recombinant TNAP protein does not rescue craniosynostosis [26,
282 47]. While lentiviral TNAP treatment did not rescue cranial base synchondrosis fusion in the
283 Crouzon mice, length of the pre-sphenoid bone was increased in treated mice on the BALB/c
284 genetic background. This result is consistent with our previous study using archival lots of the
285 lentivirus [45] which suggested changes in inferior skull morphology and may indicate that

286 TNAP can promote cranial base growth in more moderate presentations of Crouzon syndrome
287 to some extent.

288 Lack of rescue of craniosynostosis, cranial base synchondrosis fusions and craniofacial shape
289 abnormalities by lentiviral delivery of mineral targeted TNAP indicates that TNAP is not
290 essential for these characteristics of Crouzon syndrome. This could be due to the fact that TNAP
291 levels are not decreased at all stages in $FGFR2^{C342Y/+}$ mice [44] and is consistent with our finding
292 in this study that serum AP levels are similar in untreated Crouzon and wild type mice. It is also
293 possible that TNAP is simply not efficacious for preventing FGFR-associated cranial bone and
294 cranial base bone fusions, despite being decreased in cranial bone progenitor cells [14, 15].
295 More recently we showed that TNAP regulates expression of FGFR2 and Erk1,2 activity [48].
296 This latter data suggests the alternative hypothesis that FGF and Erk1,2 signaling changes cause
297 craniosynostosis in TNAP deficiency as opposed to TNAP deficiency causing craniosynostosis in
298 Crouzon syndrome.

299

300 **Acknowledgments**

301 Lentiviral vector encoding the mineral targeted form of TNAP was generously provided by Dr.
302 José Luis Millán (Sanford Burnham Prebys Medical Discovery Institute, Human Genetics
303 Program, San Jose, CA).

304

305

306 References

- 307 1. Flapper WJ, Anderson PJ, Roberts RM, David DJ. Intellectual outcomes following protocol
308 management in Crouzon, Pfeiffer, and Muenke syndromes. *J Craniofac Surg.* 2009;20(4):1252-5.
309 Epub 2009/07/25. doi: 10.1097/SCS.0b013e3181acdf9a. PubMed PMID: 19625842.
- 310 2. McCarthy JG, Warren SM, Bernstein J, Burnett W, Cunningham ML, Edmond JC, et al.
311 Parameters of care for craniosynostosis. *Cleft Palate Craniofac J.* 2012;49 Suppl:1S-24S. Epub
312 2011/08/19. doi: 10.1597/11-138. PubMed PMID: 21848431.
- 313 3. Morriss-Kay GM, Wilkie AO. Growth of the normal skull vault and its alteration in
314 craniosynostosis: insights from human genetics and experimental studies. *J Anat.*
315 2005;207(5):637-53. Epub 2005/11/30. doi: 10.1111/j.1469-7580.2005.00475.x. PubMed PMID:
316 16313397; PubMed Central PMCID: PMCPMC1571561.
- 317 4. Okajima K, Robinson LK, Hart MA, Abuelo DN, Cowan LS, Hasegawa T, et al. Ocular anterior
318 chamber dysgenesis in craniosynostosis syndromes with a fibroblast growth factor receptor 2
319 mutation. *Am J Med Genet.* 1999;85(2):160-70. Epub 1999/07/16. PubMed PMID: 10406670.
- 320 5. Rasmussen SA, Yazdy MM, Frias JL, Honein MA. Priorities for public health research on
321 craniosynostosis: summary and recommendations from a Centers for Disease Control and
322 Prevention-sponsored meeting. *Am J Med Genet A.* 2008;146A(2):149-58. Epub 2007/12/15.
323 doi: 10.1002/ajmg.a.32106. PubMed PMID: 18080327.
- 324 6. Seruya M, Oh AK, Boyajian MJ, Posnick JC, Keating RF. Treatment for delayed presentation
325 of sagittal synostosis: challenges pertaining to occult intracranial hypertension. *J Neurosurg*
326 *Pediatr.* 2011;8(1):40-8. Epub 2011/07/05. doi: 10.3171/2011.4.PEDS1160. PubMed PMID:
327 21721888.
- 328 7. Abe H, Ikota T, Akino M, Kitami K, Tsuru M. Functional prognosis of surgical treatment of
329 craniosynostosis. *Childs Nerv Syst.* 1985;1(1):53-61. Epub 1985/01/01. PubMed PMID: 3986842.
- 330 8. Baird LC, Gonda D, Cohen SR, Evers LH, LeFloch N, Levy ML, et al. Craniofacial reconstruction
331 as a treatment for elevated intracranial pressure. *Childs Nerv Syst.* 2012;28(3):411-8. Epub
332 2011/11/10. doi: 10.1007/s00381-011-1615-6. PubMed PMID: 22068642.
- 333 9. Renier D, Lajeunie E, Arnaud E, Marchac D. Management of craniosynostoses. *Childs Nerv*
334 *Syst.* 2000;16(10-11):645-58. Epub 2001/01/11. doi: 10.1007/s003810000320. PubMed PMID:
335 11151714.
- 336 10. Chen L, Li D, Li C, Engel A, Deng CX. A Ser252Trp [corrected] substitution in mouse fibroblast
337 growth factor receptor 2 (Fgfr2) results in craniosynostosis. *Bone.* 2003;33(2):169-78. Epub
338 2003/09/23. PubMed PMID: 14499350.
- 339 11. Deckelbaum RA, Holmes G, Zhao Z, Tong C, Basilico C, Loomis CA. Regulation of cranial
340 morphogenesis and cell fate at the neural crest-mesoderm boundary by engrailed 1.
341 *Development.* 2012;139(7):1346-58. Epub 2012/03/08. doi: 10.1242/dev.076729. PubMed
342 PMID: 22395741; PubMed Central PMCID: PMCPMC3294437.
- 343 12. Eswarakumar VP, Horowitz MC, Locklin R, Morriss-Kay GM, Lonai P. A gain-of-function
344 mutation of Fgfr2c demonstrates the roles of this receptor variant in osteogenesis. *Proc Natl*
345 *Acad Sci U S A.* 2004;101(34):12555-60. Epub 2004/08/19. doi: 10.1073/pnas.0405031101.
346 PubMed PMID: 15316116; PubMed Central PMCID: PMCPMC515096.

- 347 13. Holmes G, Rothschild G, Roy UB, Deng CX, Mansukhani A, Basilico C. Early onset of
348 craniosynostosis in an Apert mouse model reveals critical features of this pathology. *Dev Biol.*
349 2009;328(2):273-84. Epub 2009/04/25. doi: 10.1016/j.ydbio.2009.01.026. PubMed PMID:
350 19389359; PubMed Central PMCID: PMCPMC2674120.
- 351 14. Liu J, Kwon TG, Nam HK, Hatch NE. Craniosynostosis-associated Fgfr2(C342Y) mutant bone
352 marrow stromal cells exhibit cell autonomous abnormalities in osteoblast differentiation and
353 bone formation. *Biomed Res Int.* 2013;2013:292506. Epub 2013/06/14. doi:
354 10.1155/2013/292506. PubMed PMID: 23762837; PubMed Central PMCID: PMCPMC3665166.
- 355 15. Liu J, Nam HK, Wang E, Hatch NE. Further analysis of the Crouzon mouse: effects of the
356 FGFR2(C342Y) mutation are cranial bone-dependent. *Calcif Tissue Int.* 2013;92(5):451-66. Epub
357 2013/01/30. doi: 10.1007/s00223-013-9701-2. PubMed PMID: 23358860; PubMed Central
358 PMCID: PMCPMC3631296.
- 359 16. McGee-Lawrence ME, Li X, Bledsoe KL, Wu H, Hawse JR, Subramaniam M, et al. Runx2
360 protein represses Axin2 expression in osteoblasts and is required for craniosynostosis in Axin2-
361 deficient mice. *J Biol Chem.* 2013;288(8):5291-302. Epub 2013/01/10. doi:
362 10.1074/jbc.M112.414995. PubMed PMID: 23300083; PubMed Central PMCID:
363 PMCPMC3581413.
- 364 17. Merrill AE, Bochukova EG, Brugger SM, Ishii M, Pilz DT, Wall SA, et al. Cell mixing at a neural
365 crest-mesoderm boundary and deficient ephrin-Eph signaling in the pathogenesis of
366 craniosynostosis. *Hum Mol Genet.* 2006;15(8):1319-28. Epub 2006/03/17. doi:
367 10.1093/hmg/ddl052. PubMed PMID: 16540516.
- 368 18. Miraoui H, Marie PJ. Pivotal role of Twist in skeletal biology and pathology. *Gene.*
369 2010;468(1-2):1-7. Epub 2010/08/11. doi: 10.1016/j.gene.2010.07.013. PubMed PMID:
370 20696219.
- 371 19. Rice DP, Connor EC, Veltmaat JM, Lana-Elola E, Veistinen L, Tanimoto Y, et al. Gli3Xt-J/Xt-J
372 mice exhibit lambdoid suture craniosynostosis which results from altered osteoprogenitor
373 proliferation and differentiation. *Hum Mol Genet.* 2010;19(17):3457-67. Epub 2010/06/24. doi:
374 10.1093/hmg/ddq258. PubMed PMID: 20570969; PubMed Central PMCID: PMCPMC2916710.
- 375 20. Rice DP, Kim HJ, Thesleff I. Apoptosis in murine calvarial bone and suture development. *Eur*
376 *J Oral Sci.* 1999;107(4):265-75. Epub 1999/09/01. PubMed PMID: 10467942.
- 377 21. Twigg SR, Kan R, Babbs C, Bochukova EG, Robertson SP, Wall SA, et al. Mutations of ephrin-
378 B1 (EFNB1), a marker of tissue boundary formation, cause craniofrontonasal syndrome. *Proc*
379 *Natl Acad Sci U S A.* 2004;101(23):8652-7. Epub 2004/05/29. doi: 10.1073/pnas.0402819101.
380 PubMed PMID: 15166289; PubMed Central PMCID: PMCPMC423250.
- 381 22. Yousfi M, Lasmoles F, El Ghouzzi V, Marie PJ. Twist haploinsufficiency in Saethre-Chotzen
382 syndrome induces calvarial osteoblast apoptosis due to increased TNFalpha expression and
383 caspase-2 activation. *Hum Mol Genet.* 2002;11(4):359-69. Epub 2002/02/21. PubMed PMID:
384 11854168.
- 385 23. Zhang X, Carpenter D, Bokui N, Soo C, Miao S, Truong T, et al. Overexpression of Nell-1, a
386 craniosynostosis-associated gene, induces apoptosis in osteoblasts during craniofacial
387 development. *J Bone Miner Res.* 2003;18(12):2126-34. Epub 2003/12/16. doi:
388 10.1359/jbmr.2003.18.12.2126. PubMed PMID: 14672347.

- 389 24. Reardon W, Winter RM, Rutland P, Pulleyn LJ, Jones BM, Malcolm S. Mutations in the
390 fibroblast growth factor receptor 2 gene cause Crouzon syndrome. *Nat Genet.* 1994;8(1):98-
391 103. Epub 1994/09/01. doi: 10.1038/ng0994-98. PubMed PMID: 7987400.
- 392 25. Wilkie AO, Slaney SF, Oldridge M, Poole MD, Ashworth GJ, Hockley AD, et al. Apert
393 syndrome results from localized mutations of FGFR2 and is allelic with Crouzon syndrome. *Nat*
394 *Genet.* 1995;9(2):165-72. Epub 1995/02/01. doi: 10.1038/ng0295-165. PubMed PMID:
395 7719344.
- 396 26. Whyte MP, Greenberg CR, Salman NJ, Bober MB, McAlister WH, Wenkert D, et al. Enzyme-
397 replacement therapy in life-threatening hypophosphatasia. *N Engl J Med.* 2012;366(10):904-13.
398 Epub 2012/03/09. doi: 10.1056/NEJMoa1106173. PubMed PMID: 22397652.
- 399 27. Collmann H, Mornet E, Gattenlohner S, Beck C, Girschick H. Neurosurgical aspects of
400 childhood hypophosphatasia. *Childs Nerv Syst.* 2009;25(2):217-23. Epub 2008/09/05. doi:
401 10.1007/s00381-008-0708-3. PubMed PMID: 18769927.
- 402 28. Fraser D. Hypophosphatasia. *Am J Med.* 1957;22(5):730-46. Epub 1957/05/01. PubMed
403 PMID: 13410963.
- 404 29. Liu J, Nam HK, Campbell C, Gasque KC, Millan JL, Hatch NE. Tissue-nonspecific alkaline
405 phosphatase deficiency causes abnormal craniofacial bone development in the *Alpl(-/-)* mouse
406 model of infantile hypophosphatasia. *Bone.* 2014;67:81-94. Epub 2014/07/12. doi:
407 10.1016/j.bone.2014.06.040. PubMed PMID: 25014884; PubMed Central PMCID:
408 PMCPMC4149826.
- 409 30. Hatch NE, Li Y, Franceschi RT. FGF2 stimulation of the pyrophosphate-generating enzyme,
410 PC-1, in pre-osteoblast cells is mediated by RUNX2. *J Bone Miner Res.* 2009;24(4):652-62. Epub
411 2008/12/04. doi: 10.1359/jbmr.081213. PubMed PMID: 19049325; PubMed Central PMCID:
412 PMCPMC2659512.
- 413 31. Hatch NE, Nociti F, Swanson E, Bothwell M, Somerman M. FGF2 alters expression of the
414 pyrophosphate/phosphate regulating proteins, PC-1, ANK and TNAP, in the calvarial
415 osteoblastic cell line, MC3T3E1(C4). *Connect Tissue Res.* 2005;46(4-5):184-92. Epub
416 2006/03/21. doi: 10.1080/03008200500237203. PubMed PMID: 16546821.
- 417 32. Liu J, Campbell C, Nam HK, Caron A, Yadav MC, Millan JL, et al. Enzyme replacement for
418 craniofacial skeletal defects and craniosynostosis in murine hypophosphatasia. *Bone.*
419 2015;78:203-11. Epub 2015/05/12. doi: 10.1016/j.bone.2015.05.005. PubMed PMID:
420 25959417; PubMed Central PMCID: PMCPMC4466206.
- 421 33. Nishioka T, Tomatsu S, Gutierrez MA, Miyamoto K, Trandafirescu GG, Lopez PL, et al.
422 Enhancement of drug delivery to bone: characterization of human tissue-nonspecific alkaline
423 phosphatase tagged with an acidic oligopeptide. *Mol Genet Metab.* 2006;88(3):244-55. Epub
424 2006/04/18. doi: 10.1016/j.ymgme.2006.02.012. PubMed PMID: 16616566; PubMed Central
425 PMCID: PMCPMC2587042.
- 426 34. Millan JL, Narisawa S, Lemire I, Loisel TP, Boileau G, Leonard P, et al. Enzyme replacement
427 therapy for murine hypophosphatasia. *J Bone Miner Res.* 2008;23(6):777-87. Epub 2007/12/19.
428 doi: 10.1359/jbmr.071213. PubMed PMID: 18086009; PubMed Central PMCID:
429 PMCPMC2652241.
- 430 35. Yadav MC, Lemire I, Leonard P, Boileau G, Blond L, Beliveau M, et al. Dose response of
431 bone-targeted enzyme replacement for murine hypophosphatasia. *Bone.* 2011;49(2):250-6.

- 432 Epub 2011/04/05. doi: 10.1016/j.bone.2011.03.770. PubMed PMID: 21458605; PubMed Central
433 PMCID: PMCPMC3117961.
- 434 36. Meganck JA, Kozloff KM, Thornton MM, Broski SM, Goldstein SA. Beam hardening artifacts
435 in micro-computed tomography scanning can be reduced by X-ray beam filtration and the
436 resulting images can be used to accurately measure BMD. *Bone*. 2009;45(6):1104-16. Epub
437 2009/08/05. doi: 10.1016/j.bone.2009.07.078. PubMed PMID: 19651256; PubMed Central
438 PMCID: PMCPMC2783193.
- 439 37. Umoh JU, Sampaio AV, Welch I, Pitelka V, Goldberg HA, Underhill TM, et al. In vivo micro-CT
440 analysis of bone remodeling in a rat calvarial defect model. *Phys Med Biol*. 2009;54(7):2147-61.
441 Epub 2009/03/17. doi: 10.1088/0031-9155/54/7/020. PubMed PMID: 19287088.
- 442 38. Perlyn CA, DeLeon VB, Babbs C, Govier D, Burell L, Darvann T, et al. The craniofacial
443 phenotype of the Crouzon mouse: analysis of a model for syndromic craniosynostosis using
444 three-dimensional MicroCT. *Cleft Palate Craniofac J*. 2006;43(6):740-8. Epub 2006/11/16. doi:
445 10.1597/05-212. PubMed PMID: 17105336.
- 446 39. Richtsmeier JT, Baxter LL, Reeves RH. Parallels of craniofacial maldevelopment in Down
447 syndrome and Ts65Dn mice. *Dev Dyn*. 2000;217(2):137-45. Epub 2000/03/08. doi:
448 10.1002/(SICI)1097-0177(200002)217:2<137::AID-DVDY1>3.0.CO;2-N. PubMed PMID:
449 10706138.
- 450 40. Nam HK, Sharma M, Liu J, Hatch NE. Tissue Nonspecific Alkaline Phosphatase (TNAP)
451 Regulates Cranial Base Growth and Synchronosis Maturation. *Front Physiol*. 2017;8:161. Epub
452 2017/04/06. doi: 10.3389/fphys.2017.00161. PubMed PMID: 28377728; PubMed Central
453 PMCID: PMCPMC5359511.
- 454 41. Galvin BD, Hart KC, Meyer AN, Webster MK, Donoghue DJ. Constitutive receptor activation
455 by Crouzon syndrome mutations in fibroblast growth factor receptor (FGFR)2 and FGFR2/Neu
456 chimeras. *Proc Natl Acad Sci U S A*. 1996;93(15):7894-9. Epub 1996/07/23. PubMed PMID:
457 8755573; PubMed Central PMCID: PMCPMC38845.
- 458 42. Neilson KM, Friesel RE. Constitutive activation of fibroblast growth factor receptor-2 by a
459 point mutation associated with Crouzon syndrome. *J Biol Chem*. 1995;270(44):26037-40. Epub
460 1995/11/03. PubMed PMID: 7592798.
- 461 43. Robertson SC, Meyer AN, Hart KC, Galvin BD, Webster MK, Donoghue DJ. Activating
462 mutations in the extracellular domain of the fibroblast growth factor receptor 2 function by
463 disruption of the disulfide bond in the third immunoglobulin-like domain. *Proc Natl Acad Sci U S*
464 *A*. 1998;95(8):4567-72. Epub 1998/05/16. PubMed PMID: 9539778; PubMed Central PMCID:
465 PMCPMC22530.
- 466 44. Pfaff MJ, Xue K, Li L, Horowitz MC, Steinbacher DM, Eswarakumar JVP. FGFR2c-mediated
467 ERK-MAPK activity regulates coronal suture development. *Dev Biol*. 2016;415(2):242-50. Epub
468 2016/04/02. doi: 10.1016/j.ydbio.2016.03.026. PubMed PMID: 27034231; PubMed Central
469 PMCID: PMCPMC5580088.
- 470 45. Wang E, Nam HK, Liu J, Hatch NE. The effects of tissue-non-specific alkaline phosphatase
471 gene therapy on craniosynostosis and craniofacial morphology in the FGFR2C342Y/+ mouse
472 model of Crouzon craniosynostosis. *Orthod Craniofac Res*. 2015;18 Suppl 1:196-206. Epub
473 2015/04/14. doi: 10.1111/ocr.12080. PubMed PMID: 25865549; PubMed Central PMCID:
474 PMCPMC4396711.

- 475 46. Yamamoto S, Orimo H, Matsumoto T, Iijima O, Narisawa S, Maeda T, et al. Prolonged
476 survival and phenotypic correction of *Akp2*(-/-) hypophosphatasia mice by lentiviral gene
477 therapy. *J Bone Miner Res.* 2011;26(1):135-42. Epub 2010/08/06. doi: 10.1002/jbmr.201.
478 PubMed PMID: 20687159; PubMed Central PMCID: PMC3179312.
- 479 47. Whyte MP, Simmons JH, Moseley S, Fujita KP, Bishop N, Salman NJ, et al. Asfotase alfa for
480 infants and young children with hypophosphatasia: 7 year outcomes of a single-arm, open-
481 label, phase 2 extension trial. *Lancet Diabetes Endocrinol.* 2018. Epub 2018/12/19. doi:
482 10.1016/S2213-8587(18)30307-3. PubMed PMID: 30558909.
- 483 48. Nam HK, Vesela I, Siismets E, Hatch NE. Tissue nonspecific alkaline phosphatase promotes
484 calvarial progenitor cell cycle progression and cytokinesis via *Erk1,2*. *Bone.* 2018;120:125-36.
485 Epub 2018/10/21. doi: 10.1016/j.bone.2018.10.013. PubMed PMID: 30342227.
- 486

487

488

Figure Legends:

489

490 **Figure 1. Micro CT images of BALB/c congenic untreated and treated $FGFR2^{C342Y/+}$ mice.** Micro
491 CT isosurface images of P28 $FGFR2^{C342Y/+}$ Crouzon (CZ) and wild type (WT) mice on the BALB/c
492 congenic background are shown in axial view from above (A,B,C) and lateral view (B,D,F).
493 Darker bone is bone of diminished density.

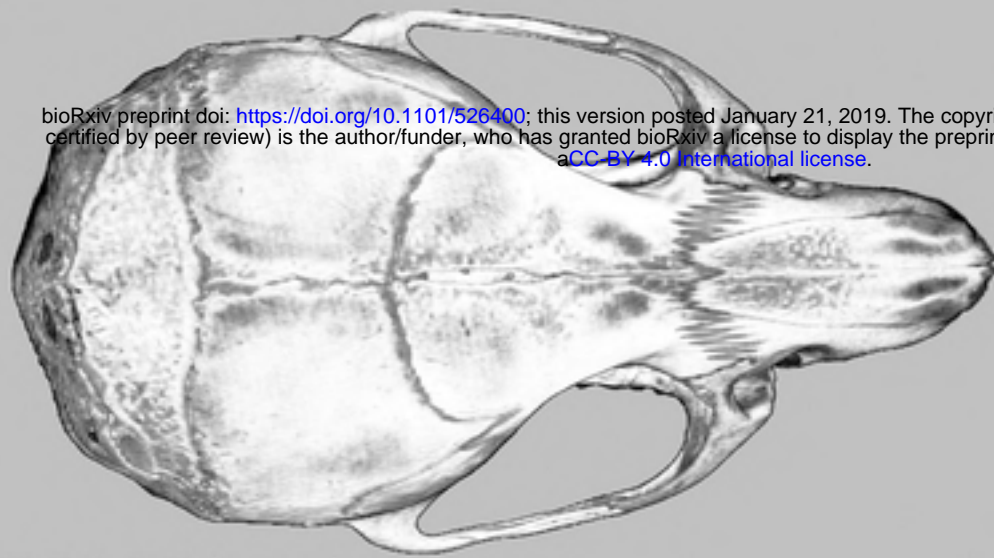
494

495 **Figure 2. Micro CT images of C57BL/6 congenic untreated and treated $FGFR2^{C342Y/+}$ mice.** Micro
496 CT isosurface images of P21 $FGFR2^{C342Y/+}$ Crouzon (CZ) and wild type (WT) mice on the C57BL/6
497 congenic background are shown in axial view from above (A,B,C) and lateral view (B,D,F).
498 Darker bone is bone of diminished density. Cranial bone density is diminished in C57BL/6
499 $FGFR2^{C342Y/+}$ mice to the extent that cranial base bones show through the translucent cranial
500 bones.

501

502 **Figure 3. Incidence of craniosynostosis and cranial base synchondrosis fusions in untreated**
503 **and treated FGFR2^{C342Y/+} mice.** No fusions are evident in wild type mice on either the BALB/c or
504 C57BL/6 backgrounds. A high incidence of coronal and lamboid suture fusion but no fusion of
505 the sagittal suture is evident in Crouzon mice on both the BALB/c and C57BL/6 backgrounds. A
506 high incidence of intersphenoidal synchondrosis (ISS) is seen in Crouzon mice on both
507 backgrounds. Speno-occipital synchondronsis (SOS) is seen approximately half of C57BL/6
508 Crouzon mice but rarely in BALB/c Crouzon mice. Treatment with TNAP does not significantly
509 influence fusion of any cranial suture or cranial base synchondroses on either genetic
510 background.

A



WT BALB/c 4wk no tx

B

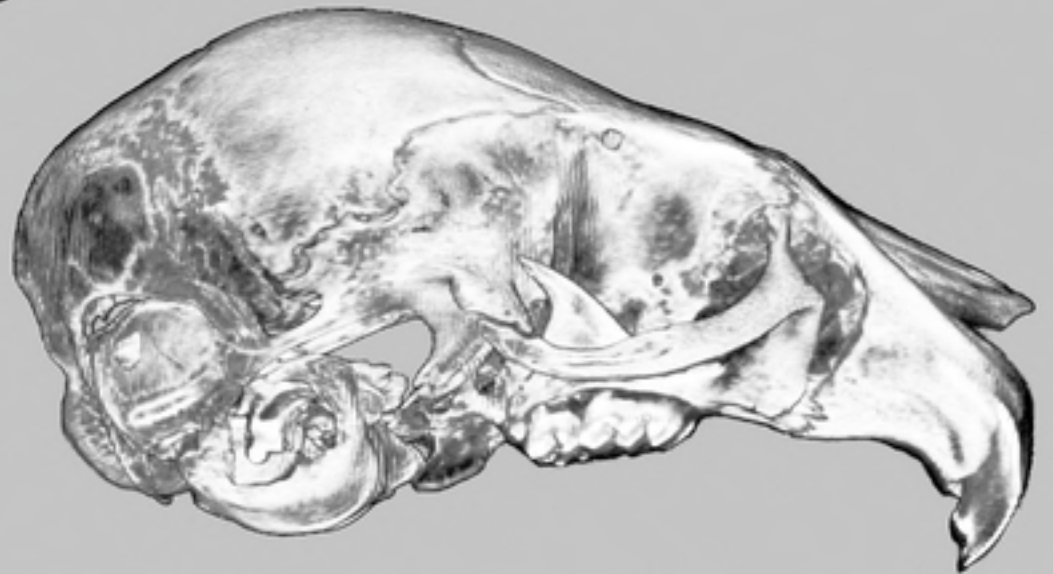


C



Cz BALB/c 4wk no tx

D



E



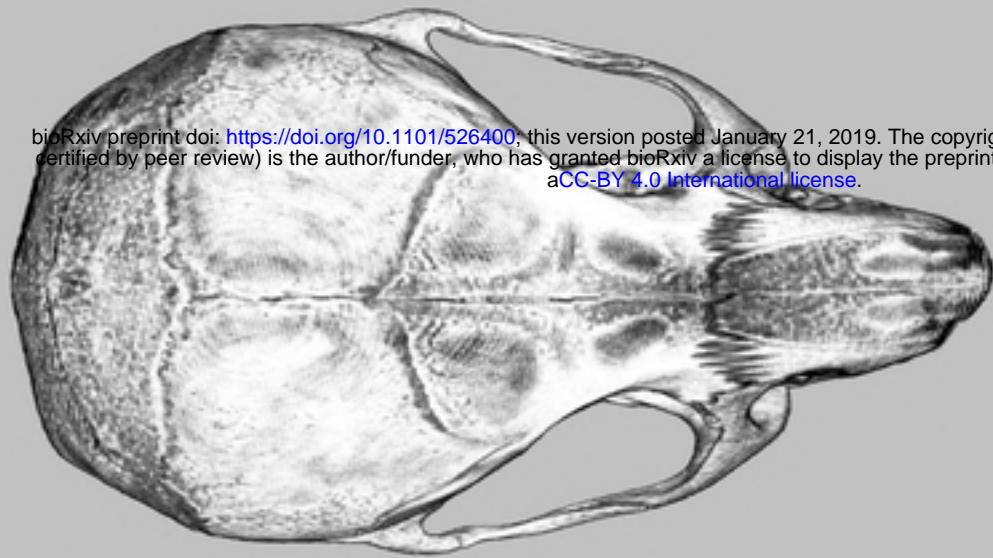
Cz BALB/c 4wk tx

F



Figure 1. Micro CT images of BALB/c congenic untreated and treated

A



WT C57BL6 3 wk no tx

B



C



Cz C57BL6 3 wk no tx

D



E



Cz C57BL6 3 wk tx

F



Figure 2. Micro CT images of C57BL/6 congenic untreated and treated

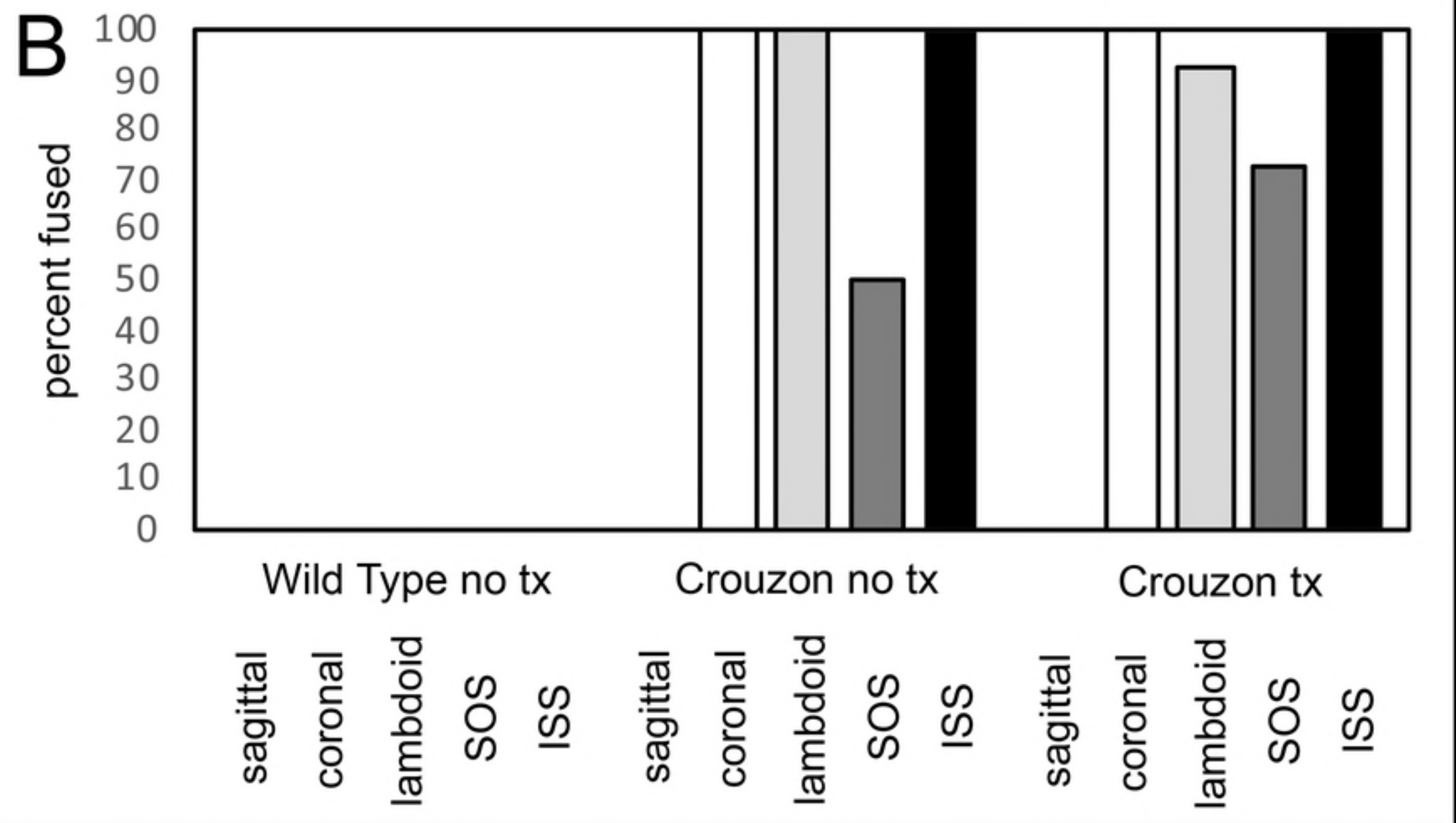
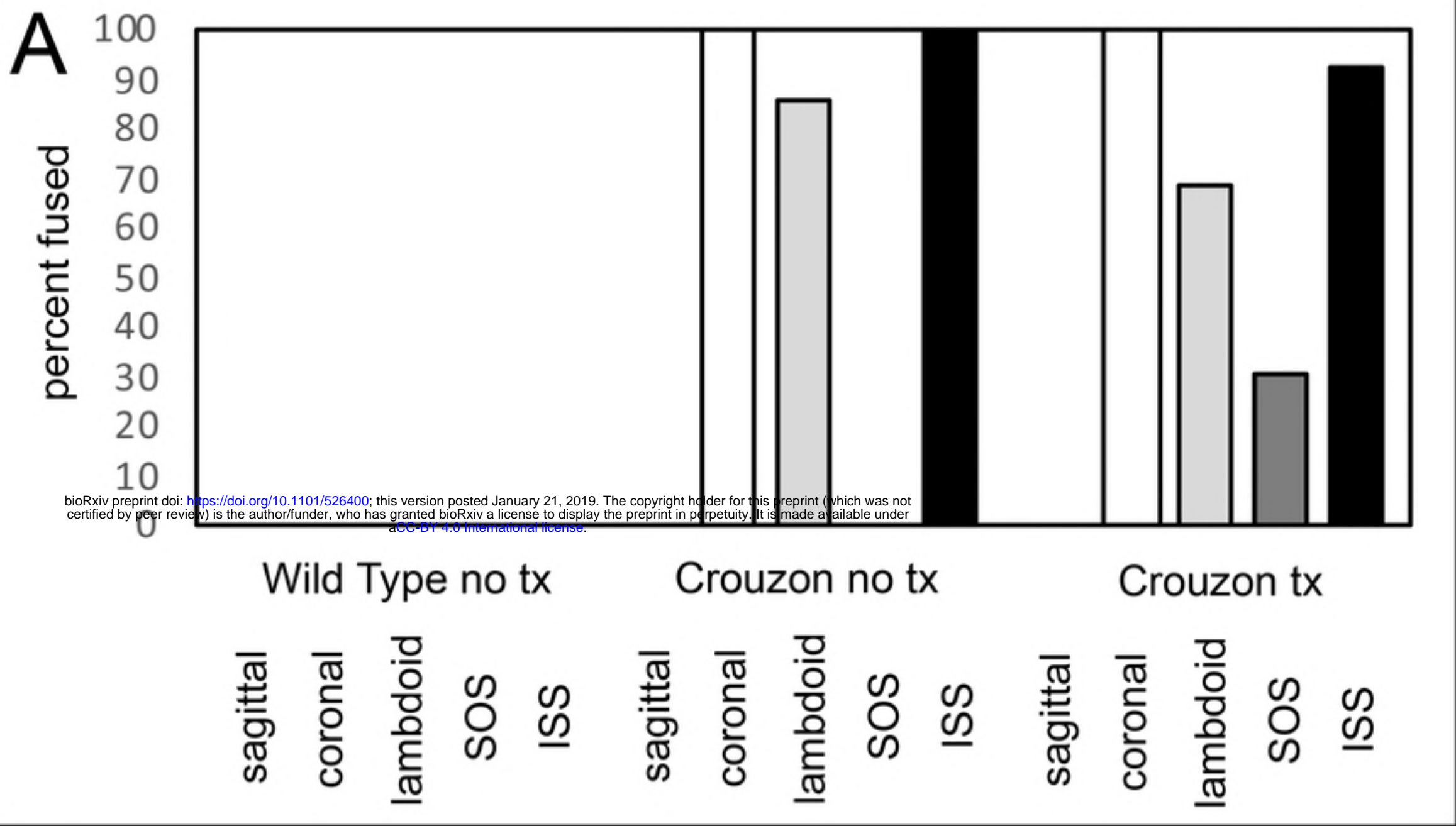


Figure 3. Incidence of craniosynostosis and cranial base synchondrosis